*Acta of Bioengineering and Biomechanics*
*Vol. 7, No. 1, 2005*

# 2D rheological models for stress relaxation and creep in living soft tissues

ALEXANDR V. KOBELEV, RIMMA M. KOBELEVA, YURIJ L. PROTSENKO

Institute of Immunology and Physiology, Russian Academy of Sciences,
Urals branch, 91 Pervomajskaja str., Ekaterinburg 620219, Russian Federation

IRINA V. BERMAN

San Jose University, Department of Physics, One Washington Square, San Jose, CA, USA

Identified rheological 2D models of myocardium proposed earlier by us to analyze static 'force-deformation' curves and quasi-static hysteresis loops are used to describe stress relaxation and creep in a wide range of living soft tissues, beginning with myocite level and up to the muscle fibers. The viscous properties are determined with the help of the dampers connected in series or in parallel to certain elastic primary elements of the models. The stress response functions of the models are found for the external longitudinal step-wise or pulse (column-like) stretching. The inverse response functions of the longitudinal displacement for the external stress loading of the pulse shape time dependencies are also found. The values of both elastic modules, as in the static case, and also viscous coefficients are estimated by comparing theoretical curves of relaxation, creep and recovery with the experimental data. The latter are obtained on rather different objects, passive muscles preparations (the stress relaxation response) and endothelium cells (the creep response). It is stated that 2D models proposed appear to be too general to describe nonlinear relaxation and creep properties, which are lacking the traditionally used 1D ones without essential modification of those models.

*Key words: soft tissues biomechanics, nonlinear viscosity, stress relaxation, creep*

## 1. Introduction

Living soft tissues on all levels of organization possess, as a rule, viscous mechanical properties due to internal viscosity of protein molecules, cytoplasmatic friction in intracellular structures, extracellular damping caused by environmental fluids, etc. The stress relaxation and the creep are considered to be the most prominent features by which this friction manifests itself in the experiments. Up untill now, they were modelled within one-dimensional (1D) rheological models similar to the four-

element Burgers–Frenkel model. These models are traced back to classical ones by Kelvin–Voigt and Maxwell [1], [2], in which the elastic (spring) and the viscose (damp) elements are connected, consequently, in parallel, or in series. The latter model and the models with the dash-pots (dampers) connected in series have been commonly believed to describe solely the stress relaxation.

Recently [3], it was pointed out that the nonlinearity of steady state and hysteretic force-length curves may be caused by a simple geometric factor involved in strained biological tissues, the so-called 'unfolding' effect of transversal vs. inclined elastic elements (see 2D models proposed therein). The possibility of an adequate description of static 'passive stress–deformation' dependence for papillary muscles was studied using classical linear elastic elements combined into the structure similar to the morphological functional unit of myocardium. The transversal elastic spring in 2D models plays an essential role hampering the unfolding and restoring the initial configuration after removal of the load.

Later [4], [5], the viscosity has been taken into account using Kelvin–Voigt blocks as inclined and transversal elements. It was found that the shape of hysteretic stress–deformation loop may indicate which elements' viscosity prevails in the sample tissue. This is straightforward to elucidate the question whether the stress relaxation can be described by the 2D models proposed. The latter may give the effects of nonlinear dependence of relaxation on deformation that is usually observed in the experiments on soft living tissues. We are also interested whether it is possible to describe the creep response, which is also nonlinear, by means of 2D models with blocks including the dampers connected in series, similar to Maxwell's model.

## 2. Morphological background

A great deal of morphological data on the living soft tissues shows definitely the similitude in the peculiarities of topological structure on the prime, secondary, tertiary, and higher levels of tissue organization. For the sake of specialization, the major part of our rheological experiments was done on a papillary muscle of laboratory animals. It has a 'cigar' shape and minor anisotropic effects, being almost uniaxial. Later we give a brief review of the myocardium morphology, having in mind the features, which are generally common both in the scale and in the kind of preparation.

Each soft biological tissue, for example, the heart muscle media (myocardium), may be partitioned into cellular and intercellular structures. Nearly one third of all cells are the myocytes, the force-producing cells in the muscle. They are connected 'end-to-end', or 'end-to-side' and make up a compound structure. According to their size, they form two third of the muscle fibers volume.

The collagen interlacing cover, which rounds the group of cells, makes the muscles elastic. It forms a complicated structure made of intercellular material, mainly the collagen threads. The collagen threads consist of tropocollagen, the triple-coiled

proper collagen molecules [6]. The spiral-shaped perimysial collagen threads form a fibrillar network, which contains the blood vessels.

The fibrillar collagen network makes up a mesh structure and consists of the struts that connect the myocites with each other, with capillaries and with large collagen filaments, or with the thin cross-connections between large collagen filaments. These struts act as the coupling springs between myocytes.

The great collagen filaments of perimysium surround the group of muscle's filaments and connect endo- and epimysium. At last, the elastic and collagen filaments envelop in a shuttle shape the continuum of some hundred of myocytes with common vessel stream in the form of a fascicule [7]. The spiral perimysium filaments couple the fascicules (the 'sheets', or the 'lamina'), and this provides compliance and sliding of the fascicules in the chamber wall.

This collagen network equalizes and aligns myocytes and capillaries, and also, prevents myocytes and sarcomers from overstretching. It also participates in the transmission of the force generated by myocytes and in providing the stretching force and stiffness of the tissue [8], [9].

The viscosity of a biological tissue on a cellular level originates from the fluid-like plasmodium cytoplasm, in which a complex system of internal cytoskeleton, made up from many intracellular microfilaments and microtubules, is immersed. The cellular membrane composed of the lipid–protein bilayer serves as a surface producing intercellular friction.

In the physiological range of deformations (within 0.3 of the sarcomer length), the static component of the stress in passive heart muscle rises nonlinearly in few cases [10], [11]. The complicated character of the 'stress–strain' relation and the dependence of dynamic differential rheological parameters on the initial conditions was found on the sheets of myocardium cardiac and skeletal muscles at sequential levels of stretching. Similar effects are observed also in the human aorta, in the skin, in sinew of the small of the back muscle, in pericardium, in brain hard cover, etc. [12]–[15].

The similarity of the morphological structures of most biological tissues makes it possible to study rheological features of various tissues using the models proposed earlier by us to describe isolated papillary muscle. Because of the complex geometry of the objects and various loading conditions, there is a need to develop 2D (and perhaps 3D) mathematical models, in addition to usually used 1D ones, in order to predict the rheological behaviour of an organ on the cellular and tissular levels.

## 3. Model description

According to the principle of a minimal number of primary elements introduced in order to simulate the rheological features observed, we use here the most primitive models depicted in figure 1. Two kinds of the problem statement will be used in the following. The description of stress relaxation is mostly pronounced when the

stepwise or rectangular pulse-shaped external stretching and releasing are given and the resulting force time is measured. On the other hand, the creep and recovery response of the total longitudinal deformation under pulse-shaped external loading can also be calculated when the external force is given and resulting deformation is calculated.

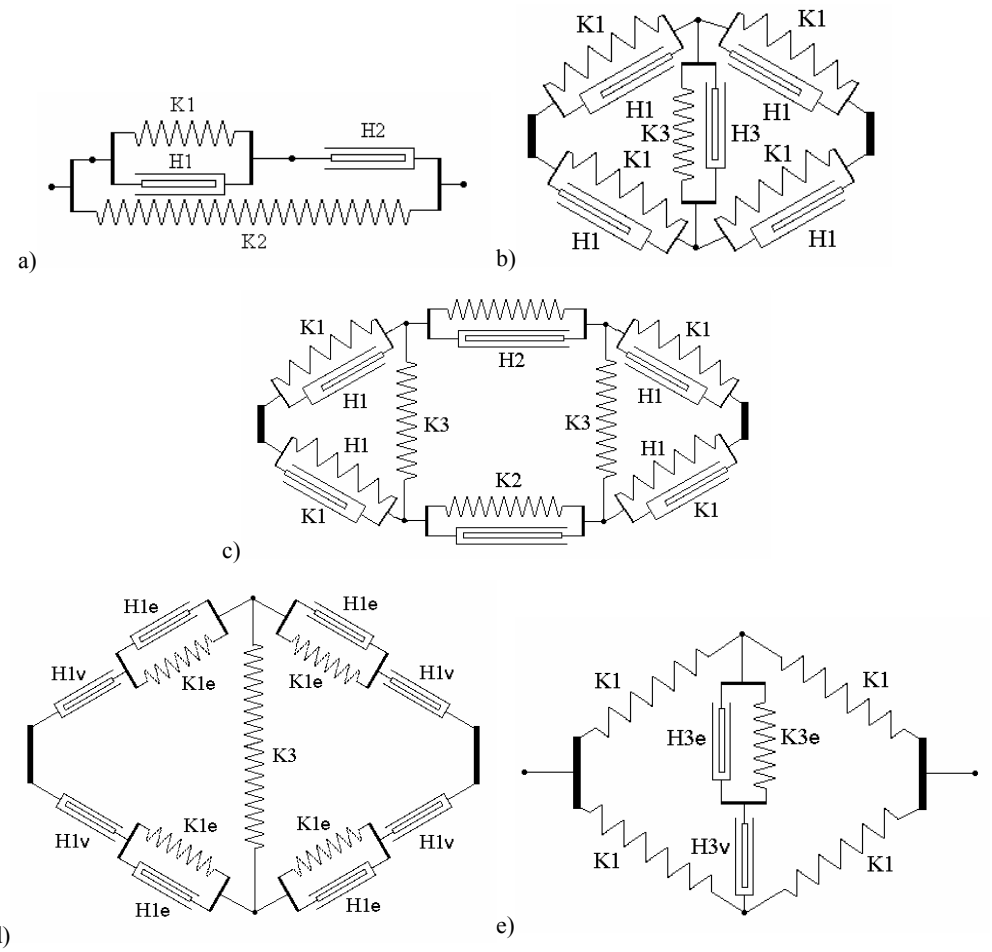


Fig. 1. Schematic view of the models composed of the elastic elements with spring elastic constants $K_i$ and damping elements with the viscous constants $H_i$, $i$ =1, 1$e$, 2, 3, 3$e$, 3$v$

The simplest 1D model KV_E (figure 1a) with four primary elements (two Hook's springs with stiffness coefficients (force/length) $K_1$, $K_2$ and two Newtonian damps (force time/length) $H_1$, $H_2$) can be solved for the resulting force $F$ acting at the right and left ends under the total external stretching with the deformation $\varepsilon(t)$ given. The

key variable in this case is the deformation $\varepsilon_2(t)$ of the damp $H_2$, which satisfies the differential equation:

$$\dot{\varepsilon}_2 = -\frac{k_1}{\eta}\varepsilon_2 + \frac{k_1}{\eta}\frac{l_0}{l_{02}}\varepsilon + \frac{\eta_1}{\eta}\frac{l_0}{l_{02}}\dot{\varepsilon}, \tag{1}$$

where the total initial length $l_0 = l_{01} + l_{02}$, hence $\varepsilon l_0 = \varepsilon_1 l_{01} + \varepsilon_2 l_{02}$, and $\eta = \eta_1 + l_{01}/l_{02}\eta_2$. Here $k_i = K_i l_{0i}$, $\eta_i = H_i l_{0i}$, $i = 1, 2$. After solving equation (1), the total force $F = k_2 f$ including both elastic and viscous components can be found:

$$f = \varepsilon + \frac{\eta_2}{k_2}\dot{\varepsilon}_2 . \tag{2}$$

The 2D rhombic model RH-K13 with Kelvin's blocks $K_1H_1$ and $K_3H_3$, whose arrangement it is shown in figure 1b, leads to the following set of differential equations in the case of the total longitudinal deformation $\varepsilon(t)$ given:

$$\dot{\varepsilon}_1 = \dot{\varepsilon}_3 \frac{\lambda_3}{\lambda_1^2}\frac{\lambda_3(1+\varepsilon_3)-\gamma}{1+\varepsilon_1} + \dot{\varepsilon}\frac{1}{\lambda_1^2}\frac{1+\varepsilon}{1+\varepsilon_1}, \tag{3}$$

$$\dot{\varepsilon}_3 = -\frac{k_2}{\eta_3}\left[1+\frac{\eta_1}{\eta_3}\frac{2\lambda_3(\lambda_3(1+\varepsilon_3)-\gamma)^2}{\lambda_1^3(1+\varepsilon_1)^2}\right]^{-1}$$
$$\cdot\left[\varepsilon_3/\kappa_3 + 2\frac{\lambda_3(1+\varepsilon_3)-\gamma}{\lambda_1(1+\varepsilon_1)}\left(\varepsilon_1/\kappa_1 + \frac{\eta_1}{k_2}\frac{1+\varepsilon}{\lambda_1^2(1+\varepsilon_1)}\dot{\varepsilon}\right)\right]. \tag{4}$$

Here the same as in (1) holds for $k_i$ and $\eta_i$, $i = 1, 2, 3$; and $\lambda_1 = 2l_{01}/l_0$, $\lambda_3 = l_{03}/l_0$, $\kappa_i = k_2/k_i$, $\gamma = h/l_0$. This set of equations for inclined ($\varepsilon_1$) and transversal ($\varepsilon_3$) deformations can be solved, giving the time dependences of these quantities, and the total force can be calculated as follows:

$$f = 2\left(\frac{\varepsilon_1}{\kappa_1} + \frac{\eta_1}{k_2}\dot{\varepsilon}_1\right)\frac{1+\varepsilon}{\lambda_1(1+\varepsilon_1)}. \tag{5}$$

Another 2D model of the 'parallelogram' geometry (figure 1c) PH-K12 represents the one which is 'flexible' at the jumps of the total longitudinal deformation. Note that the previous ones cannot be subjected to the abrupt changes in the length due to the fact that the damps are 'frozen' for infinite rate of the deformation changes. The set of differential equations for the inclined and longitudinal deformations is as follows:

$$\dot{\varepsilon}_1 = -\frac{k_2}{\eta_1}\left[\varepsilon_1/\kappa_1 + \frac{\lambda_1(1+\varepsilon_1)}{\lambda_3\kappa_3}\Psi_3\right], \tag{6}$$

$$\dot{\varepsilon}_2 = -\frac{k_2}{\eta_2}\left[\varepsilon_2 + \frac{1+\varepsilon-\lambda_2(1+\varepsilon_2)}{\lambda_3\kappa_3}\Psi_3\right], \tag{7}$$

where

$$\Psi_3 = 1 - \frac{\lambda_3 - \gamma}{\sqrt{\lambda_1^2(1+\varepsilon_1)^2 - \left[1+\varepsilon-\lambda_2(1+\varepsilon_2)\right]^2}}. \tag{8}$$

The transversal deformation can be found after solving (6) and (7) by the expression:

$$\varepsilon_3 = -1 + \frac{\gamma + \sqrt{\lambda_1^2(1+\varepsilon_1)^2 - \left[1+\varepsilon-\lambda_2(1+\varepsilon_2)\right]^2}}{\lambda_3}. \tag{9}$$

The resulting force is given by:

$$f = \left(2\varepsilon_1/\kappa_1 + 2\eta_1/k_2\,\dot{\varepsilon}_1\right)\frac{1+\varepsilon-\lambda_2(1+\varepsilon_2)}{\lambda_1(1+\varepsilon_1)}. \tag{10}$$

The last two models (figures 1d and 1e) contain the block with a damper, connected in series with the Kelvin element, in the inclined ($H_{1v}$) or in the transversal ($H_{3v}$) primary elements. They are similar to 3-element generalized Maxwell blocks in which the creep in solids and the flow in fluids are usually described. Let us present the equations for the case of a given total longitudinal deformation for the model RH-KV1 (figure 1d). The principal variables in this case are the deformations of the damper $H_{1v}$ and of Kelvin's block $H_{1e}K_{1e}$:

$$\dot{\varepsilon}_{1v} = \frac{k_{1e}}{\eta_{1v}}\varepsilon_{1e} + \frac{\eta_{1e}}{\eta_{1v}}\dot{\varepsilon}_{1e}, \tag{11}$$

$$\dot{\varepsilon}_{1e} = -\frac{k_2}{\eta_{1e}}\left[\varepsilon_{1e}/\kappa_{1e} + \frac{\lambda_1}{2\lambda_3\kappa_3}(1+1/2(\varepsilon_{1e}+\varepsilon_{1v}))\,\Theta_3\right], \tag{12}$$

where

$$\Theta_3 = 1 - \frac{\lambda_3 - \gamma}{\sqrt{\lambda_1^2[1+1/2(\varepsilon_{1e}+\varepsilon_{1v})]^2 - (1+\varepsilon)^2}}. \tag{13}$$

The resulting force can be calculated according to:

$$f = \frac{2\,\dot{\varepsilon}_{1v}\,\eta_{1v}}{k_2}\frac{1+\varepsilon}{\lambda_1[1+1/2(\varepsilon_{1e}+\varepsilon_{1v})]} \tag{14}$$

Let us now turn to the inversed statement of the problem, when the external longitudinal loading $f(t)$ is given and the resulting longitudinal deformation $\varepsilon(t)$ should be found. We begin with the model KV_E (figure 1a) already solved in the straightforward statement. Now the set of differential equations reduces to:

$$\dot{\varepsilon}_2 = \frac{k_2}{\eta_2}[f(t) - \varepsilon], \tag{15}$$

$$\dot{\varepsilon} = -\left(\frac{\eta}{\eta_1}\frac{l_{02}}{l_0}\frac{k_2}{\eta_2} + \frac{k_1}{\eta_1}\right)\varepsilon + \frac{l_{02}}{l_0}\frac{k_1}{\eta_1}\varepsilon_2 + \frac{\eta}{\eta_1}\frac{l_{02}}{l_0}\frac{k_2}{\eta_2}f(t). \tag{16}$$

In the rhombic model RH-K13 with Kelvin's viscous blocks $K_1H_1$ and $K_3H_3$ in the inclined and transversal elements (figure 1b) the following equations hold:

$$\dot{\varepsilon}_1 = -\frac{k_2}{\eta_1\kappa_1}\varepsilon_1 + \frac{k_2}{2\eta_1}\frac{f(t)}{\sqrt{1-\left[\dfrac{\lambda_3(1+\varepsilon_3)-\gamma}{\lambda_1(1+\varepsilon_1)}\right]^2}}, \tag{17}$$

$$\dot{\varepsilon}_3 = -\frac{k_2}{\eta_3\kappa_3}\varepsilon_3 - \frac{k_2}{\eta_3}\frac{[\lambda_3(1+\varepsilon_3)-\gamma]f(t)}{\sqrt{[\lambda_1(1+\varepsilon_1)]^2 - [\lambda_3(1+\varepsilon_3)-\gamma]^2}}. \tag{18}$$

The resulting total longitudinal deformation is:

$$\varepsilon = -1 + \sqrt{[\lambda_1(1+\varepsilon_1)]^2 - [\lambda_3(1+\varepsilon_3)-\gamma]^2}\ . \tag{19}$$

And at last, in the rhombic model with connected in series viscous and Kelvin's blocks as transversal element RH-KV3 (figure 1e), in the case of a given external loading $f(t)$ the set of three differential equations representing deformations of transversal viscous $\varepsilon_{3v}$, transversal elastic $\varepsilon_{3e}$ and inclined elastic $\varepsilon_1$ elements is as follows:

$$\dot{\varepsilon}_{3v} = -\frac{2k_2\lambda_3}{\lambda_1\kappa_1\eta_{3v}}(1+\varepsilon_3)\frac{\varepsilon_1}{1+\varepsilon_1}, \tag{20}$$

$$\dot{\varepsilon}_{3e} = -\frac{2k_2\lambda_3}{\lambda_1\kappa_1\eta_{3e}}(1+\varepsilon_3)\frac{\varepsilon_1}{1+\varepsilon_1} - \frac{k_{3e}}{\eta_{3e}}\varepsilon_{3e}, \tag{21}$$

$$\dot{\varepsilon}_1 = \frac{\lambda_3^2(1+\varepsilon_3)\left[\frac{k_2\lambda_3}{\eta_3\kappa_1}(1+\varepsilon_3)\frac{\varepsilon_1}{1+\varepsilon_3} - \frac{k_{3e}}{2\eta_{3e}}\varepsilon_{3e}\right] - \left(\frac{\kappa_1\lambda_1}{2}\right)^2\left(\frac{1+\varepsilon_1}{\varepsilon_1}\right)^2 f(t)\dot{f}(t)}{\lambda_1^2(1+\varepsilon_1)\left[1-\frac{\kappa_1^2}{4}\frac{f(t)^2}{\varepsilon_1^3}\right]}, \quad (22)$$

where expression (19) holds for the resulting deformation, and it is assumed that $\varepsilon_3 = 1/2(\varepsilon_{3e} + \varepsilon_{3v})$.

## 4. Results

In order to compare the model predictions with the experimental data, we have taken two works [12], [16] with rather different objects (passive muscles and endothelial cells) and different methods used and features measured (stress relaxation and creep), having in mind the generality of the phenomenological models proposed.

At first, we shall study the displacement under periodic column-like loading force in 1D and 2D models. Then it will be compared with the results of creep measurements in living cells of macrophages [16] shown in figure 2. The spatial scale of these experiments carried out with the help of micron-size magnetic beads is less than micron displacements and the forces scale is 0.4 mN in the peak of the rectangular pulse of the force applied. The magnetic bead is implanted at the surface of the cell and moves under external magnetic force. Due to different kinds of bonds, the bead moves at the same time as in a viscous fluid, and having elastic restrictions of the attached environmental filaments.

a) b)

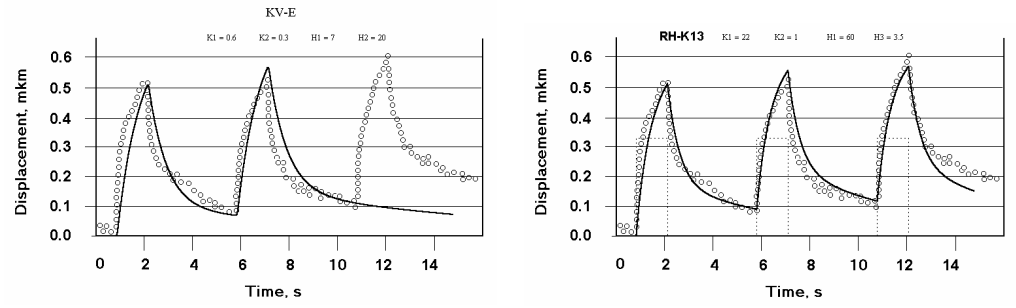


c) d)

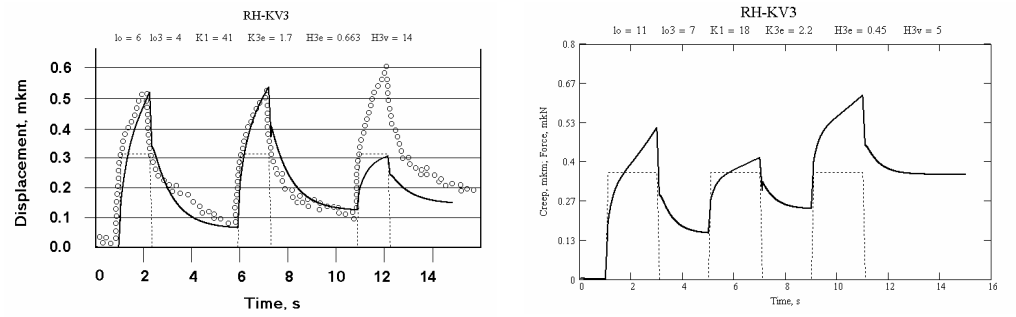


Fig. 2. The displacements at 3 periodic pulses of external force in KV-E (a), RH-K13 (b) and RH-KV1 (c) models in comparison with experimental data [16]. The values of parameters are given in the upper parts of the panels. The curve (d) represents the creep versus time with non-monotonic dependence of peak amplitude in the model RH-KV1 at some different values of parameters

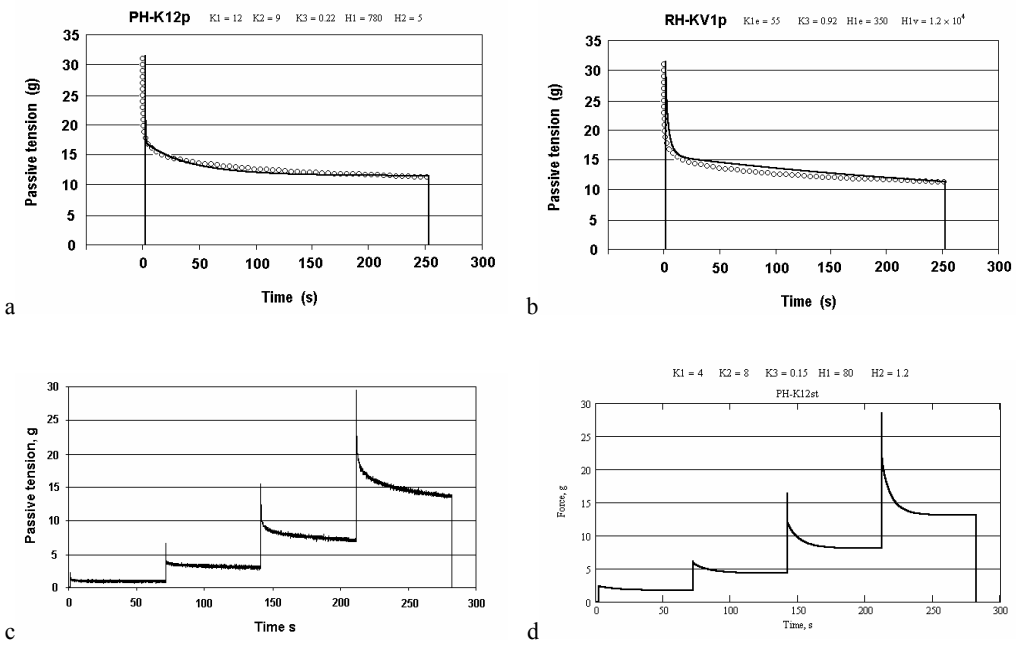


a b

c d

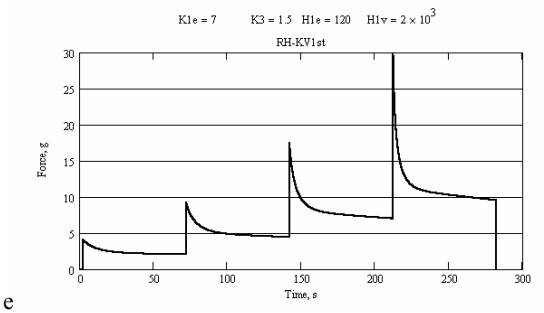


e

Fig. 3. Passive tension decay in skeletal muscle preparation [12] at longitudinal stretching $\varepsilon = 0.23$ of rectangular shape (circles) and predictions in parallelogram PH-K12 geometry (a) and rhomb RH-KV1 geometry (b) models. The time of passive tension evolution in the same preparation [12] at four-steps consequential stretching by $\varepsilon = 0.05$ in the experiment (c) and according to the predictions in the same models as in (a) and (b), respectively, (d) and (e)

Figure 2a shows the results in the 1D model from figure 1a. Although it can be usually found in the literature [12], it contradicts experimental data which is its serious drawback. Namely, the shape of the consequtive steps of the displacement curve in this model (and also in all 1D models) is one and the same, irrespective of the step number.

The result in 2D model (figure 2b) fits better the experimental data, but it appears that the unfolding effect that causes the non-linearity of stress–strain dependence and, consequently, the dependence of the curve shape on the step number, in this case, is almost beyond the range investigated.

The model with transversal block composed of damper connected in series with Kelvin's element (figure 1e) seems to be the most promising one. The displacement response curve at the second peak (figure 2c) is in quite good accord with experimental result. The second peak has slightly lower experimental amplitude than the first peak, but unfortunately, the curve fails in the amplitude and the shape of the third peak. Nevertheless, this model quite satisfactorily describes non-monotonic dependences of the peak amplitude on the pulse number due to high sensitivity of the curve shape to the values of model parameters, which is shown in figure 2d.

Now we turn to another statement of the problem, which deals with the stress relaxation under stepwise external stretching. Figure 3a presents the stress relaxation in time [12] in passive skeletal muscle, 11 mm in length, induced by stepwise extension with deformation of 0.23 compared with traces obtained in parallelogram PH-K12 (figure 3a) and rhombic RH-KV1 (figure 3b) models with two types of viscous element topology (see figures 1c and 1d, respectively). The traces are shifted to the left by 3 sec. The negative part is not shown. We can conclude that (b) shows qualitatively better fit, although one cannot definitely attribute the decrease in the stress to the relaxation (a) or to the creep (b). Experimental time of the stress at four-step increment by 0.05 in deformation, which is the other trail on the same preparation in [12], is shown in figure

3c. Note the nonlinear rise of the amplitude spikes due to the impact stiffness in the points of abrupt increments of the sample length. Here the change of relaxation rate with deformation value is also seen, which is characteristic of the most living soft tissues. The curve obtained in model b (figure 3e) is in good concordance with experimental curve in both peak tension values and decay shapes, depending on the step number, although the model (a) shows quite good fit, too (figure 3d).

## 5. Discussion

One of the physiological functions of viscosity in living tissues is to prevent their breaking at fast deformations. Practically all biological tissues are viscous; however, the nature of viscosity in muscle tissues was unclear up untill now. It is realized that the response to sufficiently quick increments of deformation in the passive muscle is accompanied by the relaxation. A number of experiments [2], [12] show that the relaxation processes are influenced not only by the amplitude of the deformation step, but also by the working length of the preparation. This effect is not reproduced in any of rheological models without additional assumption that viscosity coefficient depends on the preparation length [9].

The geometrical factor of the tissue structure may be successfully used in mathematical modelling of active [3]–[5] and passive stress dependence on the muscle length. The myocardium morphological structures, as in most of other living soft tissues, with various values of linear stiffness are functioning in different range of physiological deformations. In the initial range of deformations, soft elements are mostly involved, whose resistance to active stress generated by the muscle is weaker. When deformation increases, stiff elements play the main role preventing the tissue destruction. This fact is the key moment in our description of the nonlinear stress–strain dependencies in 2D models proposed. For example, the increasing stiffness with deformation may be caused by the ‘unfolding’ effect [3]. This is true, if certain topology with more soft transversal elastic elements and more stiff inclined and longitudinal elements is fulfilled in the tissue morphology. Thus, our proposition to go beyond the traditional linear 1D models is obviously promising in description of nonlinear rheological features of living soft tissues often observed.

The 2D models presented here offer quite good possibility of describing the most characteristic steady state, hysteretic and stress relaxation features in living soft tissues. It is so, even in the models with Kelvin’s blocks that cannot give the stress relaxation itself in 1D. These models are useful, provided that they are included in 2D models, due to an extra degree of freedom guaranteed by two-dimensionality. This way, the relation between the structure and the function manifests itself in various models corresponding to different types of the tissue morphology. The most reliable model, with respect to experimental data, may reflect the most probable and working structure of the preparation.

The non-linearity of stress–deformation relation in the case of stress relaxation leads to the dependence of the spike amplitude at the equal-step deformation on the working length determined by the step number. Moreover, for the same reason, the relaxation rate depends on the step number. In other words, this means that if the soft element with low viscosity works first, the relaxation rate will be low in the first step. Then, when the hard elements of greater viscosity predominantly start working, the relaxation rate raises in the next deformation steps. It is likely, just the same case takes place in the relaxation experiments [12].

## Acknowledgements

The authors are grateful to RFBI URALS Grant 04-04-96 109 for support.

## References

[1] VINOGRADOV G.V., MALKIN A.Ya., *The Rheology of Polymers* (in Russian), Moscow, Khimiya, 1977, 440 p.

[2] IZAKOV V.Ya., MARKHASIN B.S., YASNIKOV G.P., BELOUSOV V.C., PROTSENKO Yu.L., *Introduction to biomechanics of passive myocardium* (in Russian), Moscow, Nauka, 2000, 208 p.

[3] PROTSENKO Yu.L., KOBELEV A.V., KOBELEVA R.M., ROUTKEVICH S.M., *The steady-state property 'force–deformation' for passive myocardium*, Russian J. of Biomechanics, 2001, Vol. 5, No. 3, pp. 30–40.

[4] KOBELEV A.V., PROTSENKO Yu.L., KOBELEVA R.M., *Modeling of non-linear visco-elastic properties of myocardium specimens*, Acta of Bioengineering and Biomechanics, 2002, Vol. 4 (suppl.),
pp. 498–499.

[5] KOBELEV A.V., KOBELEVA R.M., PROTSENKO Yu.L., BERMAN I.V., *Nonlinear viscoelastic behaviour of myocardium filaments: 'force-length' hysteresis and relaxation of deformation*, Russian J. of Biomechanics, 2003, Vol. 7, No. 1, pp. 9–24.

[6] EGHBALI M., WEBER K.T., *Collagen and the myocardium: fibrillar structure, biosynthesis and degradation in relation to hypertrophy and its regression*, Mol. Cell. Biochem., 1990, 17, 96(1), pp. 1–14.

[7] GAVRISH A.S., PAUKOV V.S., *The structure and transport trophical function of the integral unit of myocardium tissue – the cardion* (in Russian), Vestnik AMN SSSR, 1988, No. 10, pp. 31–39.

[8] CAULFIELD J.B., BORG T.K., *The collagen network of the heart*, Lab. Invest., 1979, Vol. 40, pp. 364–372.

[9] WEBER K.T., BRILLA C.G., JANICKI J.S., *Myocardial fibrosis: functional significance and regulatory factors*, Cardiovasc. Res., 1993, 27, pp. 341–348.

[10] FUNG Ya.Ch., *Mathemetical models of stress–deformation relation for living soft tissues* (in Russian), Mechanics of Polymers, 1975, Vol. 5, pp. 850–867.

[11] BRAUNWALD E., ROSS J., SONNENBLICK E.H., *Mechanisms of contraction of the normal and failing heart*, Boston: Little, Brown, 1968, 205 p.

[12] ANDERSON J., LIB Z., GOUBEL F., *Models of skeletal muscle to explain the increase in passive stiffness in desmin knockout muscle*, J. Biomechanics, 2002, Vol. 35, pp. 1315–1324.

[13] DUNN M.G., SILVER F.H., *Viscoelastic behavior of human connective tissues: relative contribution of viscous and elastic components*, Connect Tissue Res., 1983, Vol. 12(1), pp. 59–70.

[14] LOEFFLER L., SAGAWA K., *A one-dimensional viscoelastic model of cat heart muscle studied by small length perturbations during isometric contraction*, Circulation Research, 1975, Vol. 36, No. 4, pp. 498–512.

[15] BRADY A.J., *Analysis of mechanical analogs of heart muscle*, Eur. J. Cardiol., 1973, Vol. 1, pp. 193–200.

[16] BAUSCH A.R., MOELLER W., SACKMANN E., *Measurement of local viscoelasticity and forces in living cells by magnetic tweezers*, Biophysical J., 1999, Vol. 76, pp. 573–579.